

Hadronic interaction at LHC: Review for the LHCf and air shower related measurements

T. Sako^{a,*}

^a*Institute for Cosmic Ray Research, University of Tokyo, Kashiwa, Chiba, Japan*

E-mail: sako@icrr.u-tokyo.ac.jp

Fifteen years have past since the first beam collisions at the Large Hadron Collider (LHC) in CERN. Not only the discovery of the Higgs particle, the LHC made a significant contribution to the cosmic-ray community. Its designed collision energy $\sqrt{s} = 14 \text{ TeV}$ corresponds to the collision of a 10^{17} eV proton on a proton at the rest frame, which is the energy range handled by the air shower observations. The particle productions in the minimum-bias events and very-forward events have been extensively measured by the various dedicated detectors at the LHC, and they serve crucial tests for the hadronic interaction models used in the cosmic-ray air shower simulations. In addition, collisions realized at various \sqrt{s} are used to test the energy evolution of the hadronic interaction. In this paper, we will review the key measurements at the LHC relevant to the air shower simulations especially focusing on the forward measurements. We will start the review from a quick outlook of some important concepts used in the high-energy and collider physics.

*7th International Symposium on Ultra High Energy Cosmic Rays (UHECR2024)
17-21 November 2024
Malargüe, Mendoza, Argentina*

*Speaker

1. Introduction

Cosmic-ray observations reach the energy beyond 10^{20} eV which is more than 7 orders of magnitude higher than the beam energy of the Large Hadron Collider (LHC) at CERN [1]. However, in terms of the collision energy in the laboratory frame, the interaction at the LHC reaches 10^{17} eV. Such high-energy controlled collisions provide important anchor points to understand the fundamental physics occurred in the development of extensive air showers (EASs). As typically demonstrated in the *muon puzzle* [2], the hadronic interaction is a crucial key to fully understand the cosmic rays through the observations of EASs. Although the major physics targets of the LHC is to search for the physics beyond the standard model and they continue challenges to increase the collision luminosity, particle production measurements in the *high-cross-section* hadronic interactions, namely *minimum bias events*, are valuable to test the hadronic interaction models implemented in the air shower simulations (*cosmic-ray models*, hereafter).

This review will start from a general description of the collider experiments for readers who are not familiar with them, including the kinematic variables and the configuration of the detectors in Sec.2 and Sec.3, respectively. Then we will outlook the important measurements made at the LHC, especially the total inelastic cross section in Sec.4 and the particle production results comparing with the cosmic-ray models in Sec.5. Among the measurements, the forward particle productions are particularly important. The major results of a dedicated forward experiment, Large Hadron Collider forward (LHCf), are focused in Sec.6. After introducing some recent topics including the forthcoming Oxygen collisions in Sec.7, the review is summarized in Sec.8.

2. Kinematics

2.1 Category of interactions

The probability of particle production is measured in terms of the cross section σ . The total cross section σ_{tot} is divided into the elastic cross section $\sigma_{elastic}$ and the inelastic cross section σ_{inela} as

$$\sigma_{total} = \sigma_{elastic} + \sigma_{inela}. \quad (1)$$

By definition, the elastic interaction does not produce new particle and the scattering angle is extremely small at high energy. This means the elastic interaction does not contribute in the EAS development. However, as discussed in Sec.4, the precise measurements of the elastic scattering at the LHC demonstrated their importance in the cosmic-ray physics.

Because the essence of the EAS development is the multi-particle production, the inelastic interaction is very important. Though there are various patterns in the inelastic interaction, a simple classification is diffractive and non-diffractive collisions. Theoretically, the diffractive collision is defined as an interaction without exchange of any quantum number, or expressed as an exchange of *Pomerons* [3]. However, in this review, we use an experimental definition or *diffractive-like* collisions, which are characterized by a wide angular gap called *rapidity gap* where no particles are produced. More phenomenologically, in the diffractive collisions, because a few particles carry most of the projectile energy, the particles are concentrated in the direction of the beam and very few or no particle are produced in the perpendicular direction. On the other hand, the non-diffractive

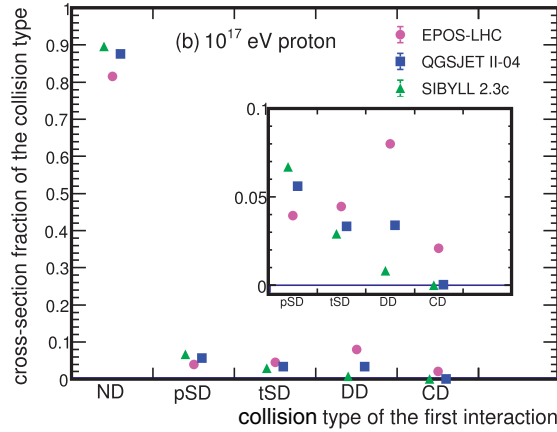


Figure 1: Cross section fraction of different processes [4]. See text for detail.

collisions produce more particles and many or most of them have large angles with respect to the beam direction. Because the produced particles widely distribute in direction and energy, the detector designs must be optimized for each process as discussed in Sec.3. The fraction of non-diffractive (ND) and diffractive collisions implemented in three cosmic-ray models are shown in Fig.1 [4]. Here the diffractive collisions are further classified into the projectile-single diffractive (pSD), target-single diffractive (tSD), double diffractive (DD) and central diffractive (CD) collisions. Though the total fraction of the diffractive cross section is 10 to 20%, because of their high energy possession as discussed in Sec.5.1 their impact on the EAS development is large.

2.2 Invariant cross section and rapidity

The angular distribution, in other words, the differential cross section $d\sigma/d\theta$ is an important quantity to be measured at the colliders. Instead of using the production (or scattering) angle of the particles, however, we usually use the kinematic variable *rapidity* (y), which is defined as,

$$y = \frac{1}{2} \ln \left(\frac{E + p_z}{E - p_z} \right),$$

where E and p_z are the total energy and the momentum along the beam direction, respectively [5]. Rapidity is defined because the differential cross section $d\sigma/dy$ is Lorentz invariant while $d\sigma/d\theta$ is not. When the relative LHC speed between the two systems along the z -direction is B in the unit of the speed of light, the rapidity in the other system y' becomes

$$y' = y + \frac{1}{2} \ln \left(\frac{1+B}{1-B} \right).$$

Though the rapidity y itself is not Lorentz invariant, its derivative y' , hence $d\sigma/dy$, becomes Lorentz invariant. Using the Lorentz invariance of the transverse momentum p_T and the relation $dy/dp_z = 1/E$, the invariant cross section containing all kinematic information is given as

$$E \frac{d^3\sigma}{d^3p} = \frac{d^3\sigma}{d\phi dy p_T dp_T} = \frac{d^2\sigma}{\pi dy d(p_T^2)}.$$

Though we find various expressions in the differential cross sections, they mean the same thing in many cases. In addition, since the total number of events observed in the experiment is given as $N = \sigma \int L dt$, where the integral is called *integral luminosity*, $d\sigma/dX$ is sometimes given as dN/dX .

2.3 Rapidity and pseudo-rapidity

In case the total energy E is sufficiently larger than the rest mass energy m , the rapidity is approximated by the *pseudo-rapidity* (η) as a function of the angle θ ,

$$y \sim \eta = -\ln \left(\tan \frac{\theta}{2} \right).$$

This is always true for photons because of $m = 0$. Here we note $\eta = 0$ for $\theta = 90^\circ$, $\eta = 1$ for $\theta = 40^\circ$, $\eta = 2$ for $\theta = 15^\circ$ and $\eta = \infty$ for $\theta = 0^\circ$. Because the determination of rapidity of each particle is practically very difficult, in many cases we use the pseudo-rapidity η as a good approximation. The rapidity range, roughly $\eta > 3$, corresponding to the forward direction is called *forward rapidity*, while the direction perpendicular to the beam is called *central rapidity*.

3. Collider setup

An illustration of the detector coverage at the LHC is shown in Fig.2. The gigantic detectors such as the ATLAS [6] and CMS [7] main detectors cover the largest solid angle around the collision point at the center of the figure as shown in the left-top of Fig.2. This coverage is important to catch the particles decayed from a heavy, rare or new particles, which are produced by converting the kinetic energy of the beam particles into the mass energy, and hence having less correlation to the beam direction. These detectors are called *central detectors* or *general purpose detectors*.

For the moderately forward particles, $\eta \sim 3$ to 6, some special detectors located close to the beam pipe and far from the interaction point are designed as shown in the right-top of Fig.2. These detectors can cover the particle production of both the diffractive and non-diffractive collisions. Because of the high detection efficiency for the various processes, the large counters in this rapidity region are called *minimum bias detectors*. The minimum bias trigger scintillators (MBTS), for example, are installed to trigger events of any type of interactions.

Because the colliders must keep the beam particles circulating, the very forward direction cannot be covered by a simple extension of the central detectors. This happens typically in the diffractive collisions. The trajectory of the charged particles produced in the very forward direction is deflected by the dipole magnet and swept away across the beam pipe. Because this happens far away from the interaction point and spread over 100's m, there is no dedicated detector installed while a special spectrometer is proposed [8]. Neutral particles, which are not deflected by the dipole magnet, can reach the crotch where the single beam pipe connecting to the interaction point is divided into two pipes connecting to the arc of the storage ring. In the gap between two beam pipes, there is a slot to install detectors as illustrated in Fig.2 left-bottom. Generally, a luminosity monitor for the accelerator operation and the Zero Degree Calorimeters (ZDC) are installed in this slot. LHCf [9] is a special type of ZDC as detailed in Sec.6. In case of the LHC, the very forward neutral particles produced in $\eta > 8.4$ are detected.

Charged particles after elastic scattering or with very little energy loss can reach the special detectors installed far away from the interaction point. The tracking detectors inserted into the vacuum beam pipe are called *Roman Pot* detectors dedicated to study the particles with extremely small scattering angles as illustrated in Fig.2 right-bottom. The TOTEM experiment [10] has dedicated Roman pot detectors in addition to the tracking detectors in the forward region. The ATLAS ALFA also makes measurements using the Roman pot detectors [11].

4. Elastic scattering measurements

Elastic cross section has an important impact on the CR modeling. An example of the TOTEM experiment is introduced here [12]. Precise measurements of the scattering angle allows the determination of $d\sigma/d|t|$ as shown in Fig.3, where t designates the momentum transfer in the collision which is directly related to the scattering angle. The integration of $d\sigma/d|t|$ gives the $\sigma_{elastic}$ with little uncertainty of the extrapolation. Also with a small extrapolation, the cross section at zero degree, $(d\sigma/d|t|)_{\theta=0}$ is determined, which gives the total cross section σ_{tot} through the Optical theorem [3]. Finally σ_{inela} is obtained through Eq.1.

Thanks to the precise measurements of σ_{inela} especially by TOTEM and ATLAS ALFA at the LHC, the large uncertainty arisen in the Tevatron era have converged. This reduces the model dependence in the energy evolution of σ_{inela} and hence converges the prediction of the elongation rate as shown in Fig.4 [13].

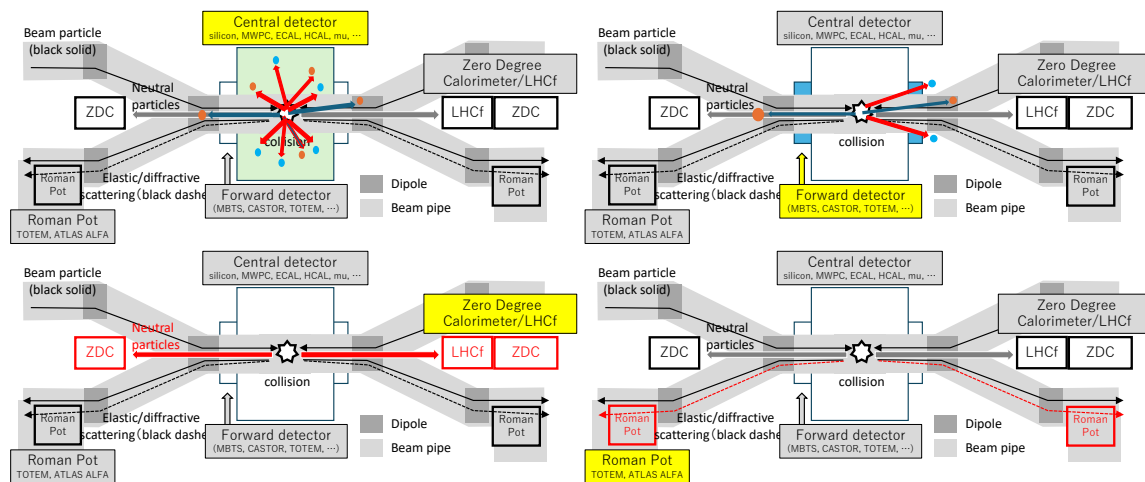


Figure 2: Detector layout at the colliders and event types they observe. (Left-top) central rapidity coverage for non-diffractive events. (Right-top) forward rapidity coverage for mixture of diffractive and non-diffractive events. (Left-bottom) neutral particle measurements at the very forward rapidity including the zero degree. (Right-bottom) coverage of elastically scattered particles.

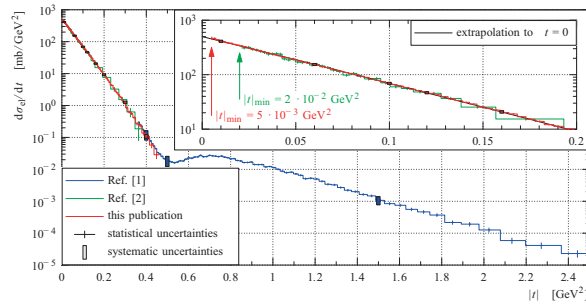


Figure 3: The TOTEM measurement of the differential elastic cross section at $\sqrt{s} = 7$ TeV [12].

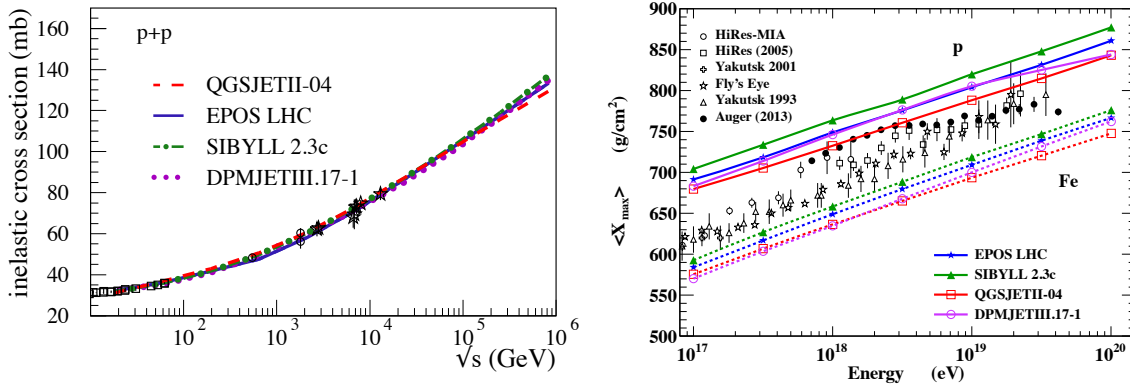


Figure 4: (Left) Inelastic cross sections measured at the LHC and the predictions by the post-LHC models. (Right) X_{max} measurements compared with the predictions by the post-LHC models [13].

5. Particle production in the inelastic collisions

5.1 Particle productions at LHC

Distributions of the particles simulated in the inelastic collisions at $\sqrt{s} = 14$ TeV as a function of η are shown in Fig.5. The left and right panels show the number of particles (multiplicity) and energy flux, respectively. It is clear that most of the particles are produced into the central rapidity while most of the energy is carried by the small number of forward particles. This means the forward particles are responsible to determine the structure of EAS core [14]. As marked in the figure, the peak of the energy flux is covered by the zero degree calorimeters introduced in Fig.2 (left-bottom) and LHCf is an experiment specially prepared for the precise measurements of the very forward particle production.

5.2 Multiplicity measurements

At the very early stage of the LHC, various measurements of minimum-bias events are compared with the model predictions. The central multiplicity measured by CMS and ALICE with the model predictions are shown in Fig.6 [15]. It was recognized, since then, the cosmic-ray models predict the results at the LHC better than the High-Energy Physics (HEP) models. The forward multiplicity

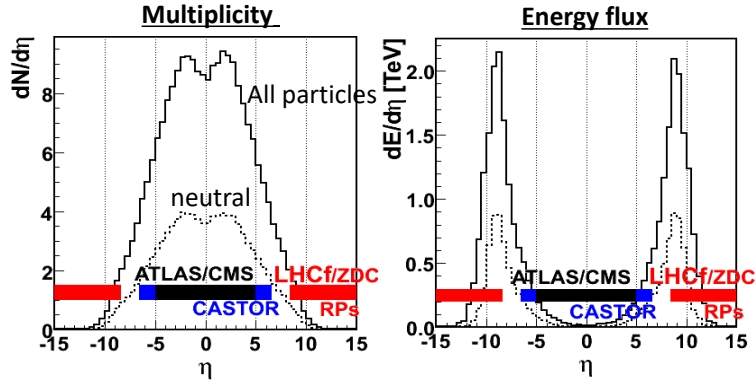


Figure 5: Rapidity distribution of the particles at the $\sqrt{s} = 14$ TeV p - p collisions. (Left) number of particles or multiplicity. (Right) energy flux carried by the particles.

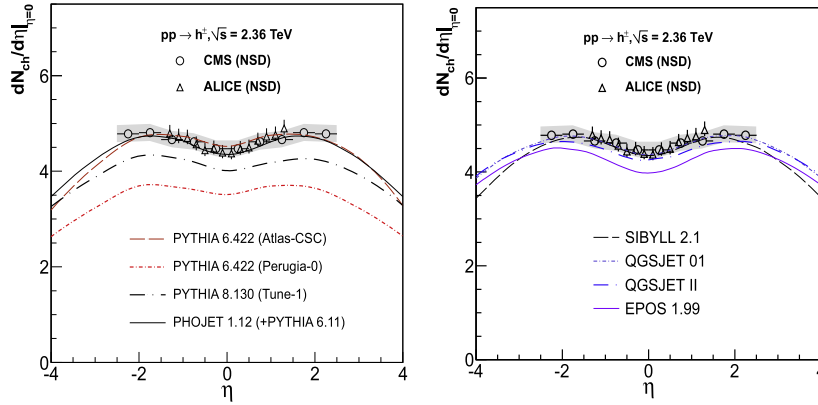


Figure 6: The pseudo-rapidity distributions measured by the CMS and ALICE experiments at $\sqrt{s} = 2.36$ TeV p - p collisions compared with (left) the HEP model predictions and (right) the cosmic-ray model predictions. Picked up from the comparisons at $\sqrt{s} = 0.9, 2.36$ and 7 TeV in [15].

at $2 < \eta < 6.4$ is measured by LHCb [16] and the CMS-TOTEM [17] as shown in Fig.7 left and right, respectively. Again it is found that the cosmic-ray models, EPOS-LHC and QGSJET II-04, reasonably describe the experimental results of CMS-TOTEM.

5.3 Energy flow measurements

The energy flow of the forward particles measured by the CMS experiment is shown in Fig.8 [18]. The left and right panels compare the experimental results with the HEP models and cosmic-ray models, respectively. It is found that the cosmic-ray models show a reasonable agreement over the rapidity range although they are so-called *pre-LHC models*. More comparisons of the forward particle measurements and *post-LHC models* by the energy spectra separated in the total, hadronic and electromagnetic components are given by using a dedicated forward calorimeter CASTOR in the CMS experiment [19].

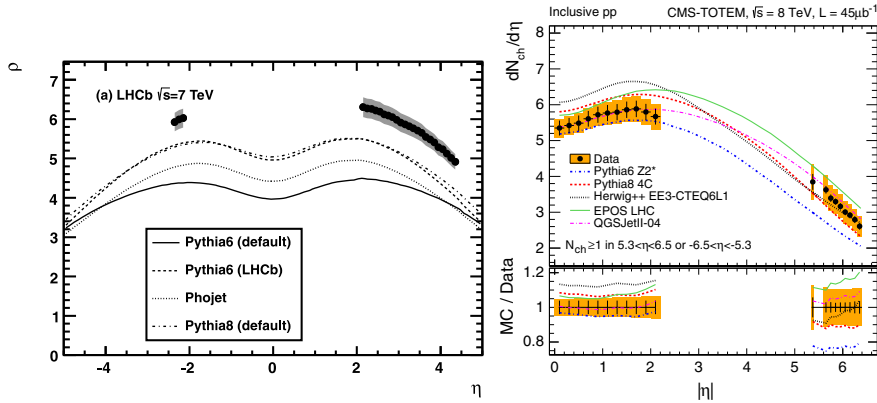


Figure 7: The pseudo-rapidity distributions measured by (left) the LHCb [16] and (right) the CMS-TOTEM experiments [17] at $\sqrt{s} = 7$ and 8 TeV, respectively. Picked up from the other comparisons with different tunes, diffractive and non-diffractive selections.

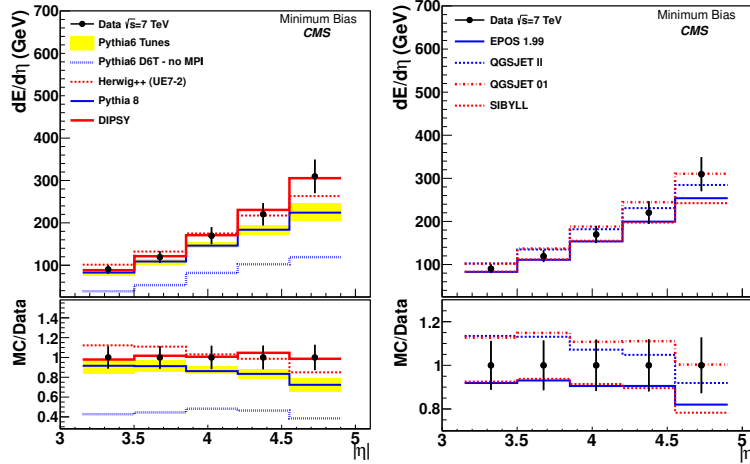


Figure 8: The energy flow of the forward particles measured by the CMS experiment [18]. Picked up from various comparisons in the different event categories and the collision energies.

6. Very forward measurements by LHCf

Here we will discuss the measurements around zero-degree focusing on the results of the LHCf experiment. LHCf installed two detectors 140 m away in either side of the ATLAS interaction point as shown in Fig.9. Each detector contains two imaging sampling calorimeters, which allow precise energy and position reconstruction of individual particle arriving at $\eta > 8.4$. Detail of the detector design and performance are described in [9] [20]. In addition, one of the LHCf detectors, Arm1, was also used to measure the forward particles at the Relativistic Heavy Ion Collider (RHIC) in the Brookhaven National Laboratory, U.S.A. as the RHICf detector [21].

At the location of the LHCf, only stable neutral particles, *i.e.*, neutrons and photons can arrive. While the neutrons carry a large fraction of the proton energy, where the fraction is called *elasticity*

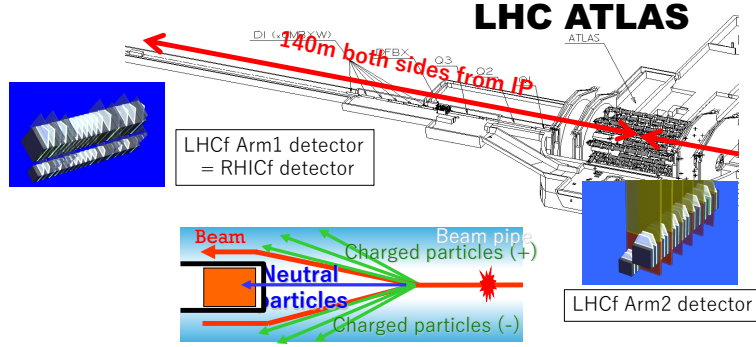


Figure 9: The location of the LHCf detectors.

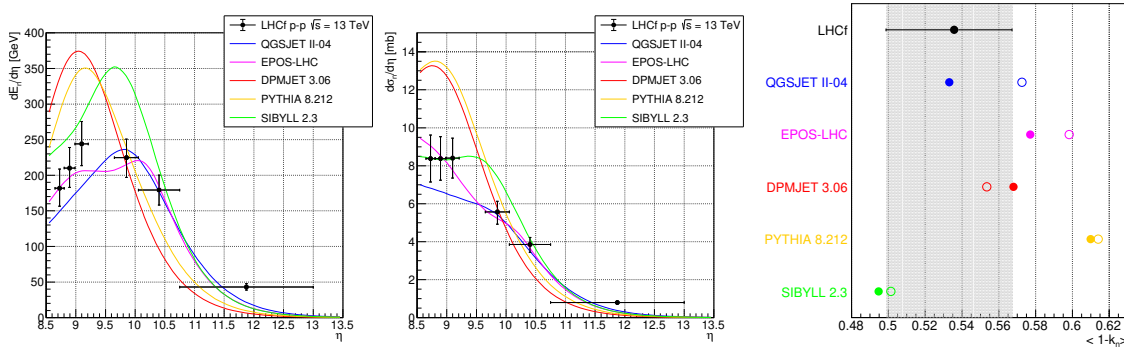


Figure 10: The energy flow (left) and multiplicity (middle) of the forward neutrons measured by LHCf. Inelasticity determined from the neutron measurements is shown in the right panel. The filled circles show the inelasticity calculated when the leading particle is neutron while the open circles are calculated whatever the leading particle is [22].

(k), the photons are mostly produced by the decay of neutral pions, whose energy distribution is characterized by the multiparticle production sharing the rest of the fractional energy $inelasticity = 1 - k$. Through the measurements of the energy spectra at 6 rapidity ranges, LHCf determined the energy flow and multiplicity of the forward neutrons as shown in Fig.10. The inelasticity ($1 - k$) is also determined and shown in Fig.10 right. The energy flow and multiplicity are well reproduced by the EPOS-LHC and QGSJET II-04 models while the other models predict larger energy flow near the peak at $\eta = 9$ to 10. Considering the experimental uncertainty, the inelasticity is well explained by the models tested here.

The neutral pions (π^0) are identified by determining the energy and impact position, hence the 4-momenta, of photons, and reconstructing the invariant mass of the photon pairs. Fig.11 shows the invariant mass distribution measured by the LHCf experiment [23]. A clear peak at 135 MeV corresponds to the photon pair events decayed from π^0 's produced at the interaction point. By summing up the momenta of the photon pair, the cross section of π^0 production in $\sqrt{s} = 7$ TeV p - p collisions is reconstructed as shown in Fig.12 [24]. Here the results are compared with the post-LHC cosmic-ray models and they are well bracketed by the predictions by EPOS-LHC (magenta)

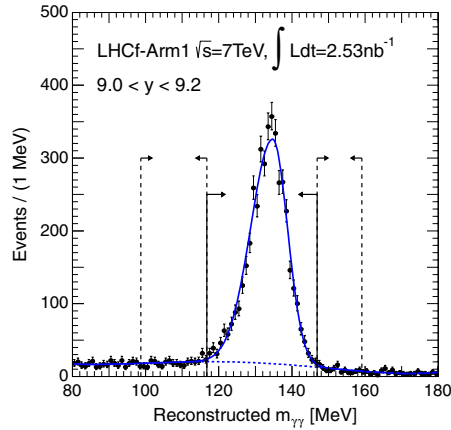


Figure 11: The invariant mass distribution of the photon pairs observed by the LHCf Arm1 detector [23].

and QGSJET II-04 (blue), which are commonly used in the EAS simulations. In more detail, it is found that EPOS-LHC produces more π^0 's than the LHCf measurements at the highest energy while QGSJET II-04 is opposite. Because 3500 GeV is the beam energy, a finite cross section of π^0 production close to the beam energy predicts a generation of very gamma-ray-like showers by primary protons. This is an essential background in the modern ground-based gamma-ray telescopes such as the Cherenkov Telescope Array and the small difference between the models at the highest energy affects the estimate of the BG contamination into the gamma-ray shower selection as studied in [25]. Though the collision energy at the LHC is a few orders of magnitude higher than the energy of interest in the gamma-ray astronomy, it is also proved that the photon production cross sections at the LHC and the RHIC show excellent scaling in the phase space of x_F and p_T as shown by LHCf [26] and RHICf [27]. Here Feynman x_F is defined as $2|p_z|/\sqrt{s}$. The relation of the forward photon production cross section between the experimental results and the model predictions hold in the energy range of $E_{lab} = 10^{14}$ eV to $10^{16.4}$ eV. This means the π^0 production cross section shown in Fig.12 is crucial to select the relevant interaction model to predict hadronic BG into the electromagnetic shower identifications.

7. Recent topics

So far, we mainly review the results of the inclusive measurements, where we focus only on the particles of interest but ignore the other activities. Though the exclusive measurements, where we constrain the process using the all produced particles, are almost impossible, some cross sections defined under controlled condition can be defined. Also measurements at different collision energies, production cross sections of mesons except pions such as η and K connected with s -quarks are also important measurements for EAS physics. Here some recent activities are listed up.

- Scaling of the forward π^0 and forward photons are studied by LHCf [24] and RHICf [27] and using the old UA7 data [28]. They conclude a nice scaling with appropriate variables.

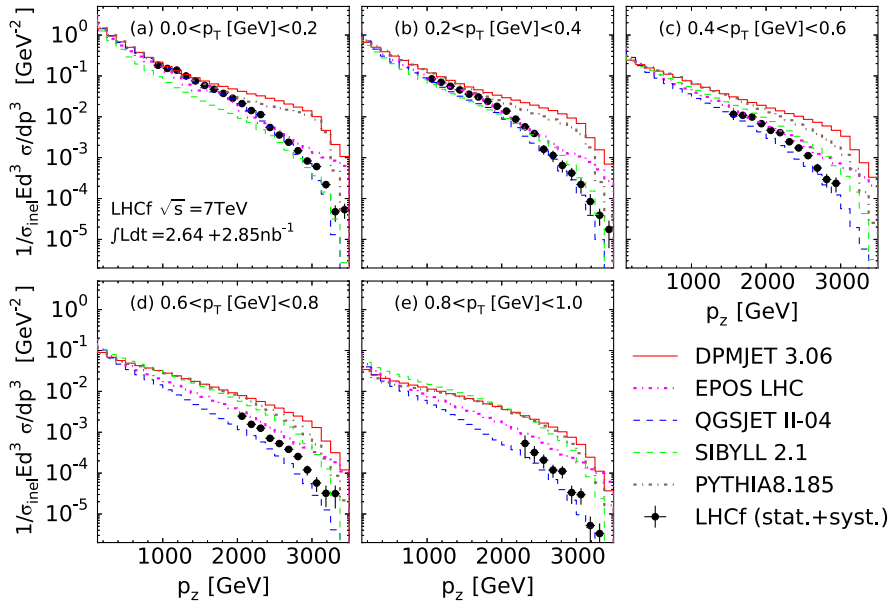


Figure 12: The differential cross sections of very forward π^0 production measured by LHCf [24]. The different panels show the results in the different p_T ranges.

- Production cross section of very forward η mesons by LHCf [29]. The model dependence larger than the π^0 case is strongly constrained by the measurement.
- Production cross section of K mesons in the central rapidity by ATLAS [30]. They measured evolution of K production as a function of the leading-jet p_T , which is related to the level of the multi-parton interaction.
- Production of strange hadrons such as K , Λ , Ξ , Ω relative to π^\pm are measured by ALICE [31]. More strange hadrons are produced as the central multiplicity increases, which means more QGP-like interaction occurs.
- The production cross sections of very-forward photons by LHCf are further classified using the information of the ATLAS central detector. The very-forward photons in the diffractive-like events, where no charged particle was observed in the central rapidity, have harder energy spectrum than the inclusive photons [32].
- Feasibility of further joint analyses between ATLAS and LHCf is studied at the MC level [33]. Phase space coverages of the interaction between the beam proton and virtual pion cloud, identification of single diffractive events using the ATLAS Forward Proton (AFP) system/ALFA and identification of Δ resonance using the AFP/ALFA and LHCf are reported.
- ALICE reported the muon bundle observation of EASs observed 80 m underground [34]. While they cannot determine the energy of the individual EAS, using MC simulation they estimated the corresponding primary energy range to be 4×10^{15} to 6×10^{16} eV. Comparing

with the cosmic-ray model predictions, they concluded the muon bundle observation suggests a heavy mass composition such as Irons in this energy region..

Finally, but most excitingly to the cosmic-ray community, the LHC decided to realize the collisions of Oxygen beams ($p-O$ and $O-O$) in 2025. While the heavy ions used at the colliders so far are Lead in LHC and Gold in RHIC, this is the first ion collisions directly relevant to simulate the cosmic-ray particles hitting the atmosphere nuclei. The impact of this measurements to the CR physics is summarized in [35]. Although, as we have seen in this review, the cosmic-ray models have been well tuned to reasonably explain the various LHC measurements, the predictions in the Oxygen collisions have still a large model dependence. This is because our knowledge of the nuclear effect, how multiple nucleons participate in a single nuclear collision, is not sufficient. As it happened 15 years ago, initial minimum-bias events coming from the LHC Oxygen collisions will make major updates of the cosmic-ray models.

8. Summary

In the past 15 years, the high-energy particle physicists recognized that the cosmic-ray models describe the LHC results very well as we have seen in this review. In the various measurements, comparisons with the cosmic-ray model predictions as well as the HEP models become a standard recipe. More dedicated analyses specifying the underlying process are ongoing. In other words, the models have more information to tune their physics implemented. In the same period, the cosmic-ray community has recognized the existence of the muon puzzle. However, even using the knowledge from the LHC, it is still an open question. The Oxygen collisions happening in 2025 will bring a break through in this situation and will be one of the most exciting and fruitful collaboration between the cosmic-ray community and the HEP community.

We also demonstrated some precise measurements of the very forward π^0 's and photons by LHCf and RHICf. These measurements are important to constrain the model uncertainties in the BG estimation of the ground-based gamma-ray observations.

References

- [1] Evans, L. and Bryant, P. (editors), JINST, 3, S08001 (2008).
- [2] Albrecht, J., Cazon, L., Dembinski, H., et al., *Astrophys. and Sp. Sci.* (2022) 367:27.
- [3] Barone, V. and Predazzi, E. "High-Energy Particle Diffraction," Springer (2001).
- [4] Ohashi, K., Menjo, H., Itow, Y., Sako, T., Kasahara, K., PTEP, 2021, 033F01.
- [5] Particle Data Group, see "Review: Kinematics." <https://pdg.lbl.gov/>.
- [6] The ATLAS Collaboration, JINST, 3, S08003 (2008).
- [7] The CMS Collaboration, JINST, 3, S08004 (2008).
- [8] Albrow, M. G., arXiv:2006.11680 (2020).

- [9] The LHCf Collaboration, JINST, 6, S08003 (2008).
- [10] The TOTEM Collaboration, JINST, 3, S08007 (2008).
- [11] The ATLAS Collaboration, Nucl. Phys. B 889 (2014) 486-548.
- [12] The TOTEM Collaboration, EPL, 101 (2013) 21002.
- [13] Pirog, T., PoS(ICRC2017)1100.
- [14] Akiba K., et al., J. Phys., G: Nucl. Part. Phys., 43 (2016) 110201; CERN-PH-LPCC-2015-001; SLAC-PUB-16364; DESY 15-167
- [15] d'Enteria, D., Engel, R., Pierog, T., Ostapchenko, S., Werner, K., Astropart. Phys. 35 (2011) 98-113.
- [16] The LHCb Collaboration, Eur. Phys. J. C (2012) 72:1847.
- [17] The CMS and TOTEM Collaborations, Eur. Phys. J. C (2014) 74:3053.
- [18] The CMS Collaboration, JHEP11(2011)148.
- [19] The CMS Collaboration, JHEP08(2017)046.
- [20] The LHCf Collaboration, IJMPA, 28 (2013) 1330036.
- [21] The RHICf Collaboration, JINST, 16, P10027 (2021).
- [22] The LHCf Collaboration, JHEP07(2020)016.
- [23] The LHCf Collaboration, PRD 86, 092001 (2012).
- [24] The LHCf Collaboration, PRD 94, 032007 (2016).
- [25] Ohishi, M., et al., J. Phys. G: Nucl. Part. Phys. 48 (2021) 075201.
- [26] The LHCf Collaboration, Phys. Lett. B 703 (2011) 128-134.
- [27] The RHICf Collaboration, arXiv:2203.15416.
- [28] The UA7 Collaboration, Phys. Lett. B 242, 531 (1990).
- [29] The LHCf Collaboration, JHEP 10 (2023) 169.
- [30] The ATLAS Collaboration, EPJC submitted; CERN-EP-2024-105 (2024).
- [31] The ALICE Collaboration, Nature Phys., 13 (2017).
- [32] The ATLAS and LHCf Collaborations, ATLAS-CONF-2017-075.
- [33] The ATLAS and LHCf Collaborations, ATL-PHYS-PUB-2023-024.
- [34] The ALICE Collaboration, arXiv:2410.17771; CERN-EP-2024-263.
- [35] Dembinski, H. P., Ulrich, R. and Pierog, T., PoS(ICRC2019)235.